Biosensors and Bioelectronics 141 (2019) 111436

Contents lists available at ScienceDirect

Biosensors and Bioelectronics

journal homepage: www.elsevier.com/locate/bios

An ultrasensitive luminol cathodic electrochemiluminescence probe with highly porous Pt on ionic liquid functionalized graphene film as platform for carcinoembryonic antigen sensing

Xiao Wang, Lei Shang*, Wei Zhang, Li-Ping Jia, Rong-Na Ma, Wen-Li Jia, Huai-Sheng Wang**

Department of Chemistry, Liaocheng University, Liaocheng, Shandong, 252059, PR China

ARTICLE INFO

Keywords:
Cathodic ECL
Porous Pt
Graphene
Immunosensor
CEA

ABSTRACT

The low-potential electrochemiluminescence (ECL) sensors based on cathodic light emission of luminol have caused more and more concerns due to their good stability and reproducibility. In this work, highly porous platinum (Pt) nanostructures on ionic liquid functionalized graphene film (GR-IL/pPt) were prepared as platform to construct a label-free ECL sensor for the detection of carcinoembryonic antigen (CEA). Due to their good biocompatibility, excellent electrocatalytic activity and highly porous structure, the as-prepared GR-IL/pPt composites benefited amplified cathodic ECL signal of luminol and high loading density of the CEA antibody. After CEA was incubated with the CEA antibody, the cathodic ECL signal of luminol decreased thanks to the less conductive immunocomplex. The proposed ECL immunosensor realized high sensitivity for CEA detection with a wide linear range from 0.001 fg mL^{-1} to 1 ng mL^{-1} and an extremely low detection limit of 0.0003 fg mL^{-1} (S/N = 3). Moreover, the sensor showed good specificity, stability and reproducibility, indicating that the provided strategy had a promising potential in clinical detection.

1. Introduction

Electrochemiluminescence (ECL) has obtained great attentions as a fast, sensitive, selective and low background analytical method (Guo et al., 2018; Li et al., 2019; Mayer et al., 2018; Rizwan et al., 2017, 2018b; Xu et al., 2018). Among the ECL systems, luminol and its derivatives are outstanding as one of the most commonly used luminophores, due to their nontoxicity, low excitation potential, chemical and thermal stability, and high luminescent efficiency (Xu et al., 2010). So far, many luminol-based ECL systems have been constructed and used in biosensing (Kitte et al., 2017; Ling et al., 2019; Qiao et al., 2018; Wang et al., 2019; Zhang et al., 2019b). For example, Zheng's group revealed that the ECL quantum yield of the luminol at the potential range from 0 to 0.5 V (vs. Ag/AgCl) on the 1,6-hexanedithiol hydrophobic pinhole film modified gold electrode was 3-fold higher than that of the bare gold electrode (Qiao et al., 2018). The increase was due to the hydrophobic microenvironment on the electrode surface, which was formed by the hydrophobic alkyl chains from their supramolecular interaction. Based on the new finding and the cap effect of gold nanoparticles to these pinhole gates, a highly sensitive ECL sensing platform for microRNA was developed. Zhang et al. developed a sensitive ECL biosensor for detection of MCF-7 exosomes using aptamer modified two-dimensional material Ti_3C_2 MXenes nanosheets as the ECL nanoprobe (Zhang et al., 2019b). Due to their unique properties such as large surface area, excellent conductivity and catalytic activity, the nanoprobe showed significantly enhanced ECL signals of luminol at the potential range of 0–0.6 V, resulting in an over 100 times lower detection limit than that of conventional ELISA method. In these examples, the biosensors were concentrated on the anodic ECL signals of luminol. However, it has been shown that luminol could produce a high cathodic light emission on the graphene (GR)-modified glassy carbon electrode at positive potential (ca. 0.05 V vs. Ag/AgCl), attributing to the promoted generation of reactive oxygen species (superoxide anion and hydroxyl radical) on the GR (Xu et al., 2011). These oxygen species could oxidize luminol into excited 3-aminophthalate dianion and finally emits lights. It was worth noting that the cathodic ECL intensity was much stronger than anodic one, so a high-efficient ECL sensor was constructed based on this cathodic signal. Besides, the low operation potential could avoid the damage of the modified electrodes and biomolecules, thus showing a good stability and reproducibility of the proposed ECL biosensor. Considering these advantages, increasing attention has been paid on the cathodic ECL signal of luminol until now

* Corresponding author.
** Corresponding author.
E-mail addresses: shanglei@lcu.edu.cn (L. Shang), hswang@lcu.edu.cn (H.-S. Wang).

https://doi.org/10.1016/j.bios.2019.111436
Received 3 April 2019; Received in revised form 3 June 2019; Accepted 11 June 2019
Available online 13 June 2019
0956-5663/

(Cao et al., 2013; Dai et al., 2012; Jiang et al., 2013). For example, gold-platinum (Au–Pt) nanoparticles (NPs) electrodeposited on GR-carbon nanotubes nanocomposite and palladium (Pd)–Pt NPs decorated GR were explored to fabricate ultrasensitive ECL immunosensors based on luminol cathodic ECL for the detection of carcinoembryonic antigen (CEA) (Cao et al., 2013). The proposed immunosensors were tested at low potential, and showed good sensitivity, selectivity and stability. Therefore, it is important and necessary to explore new GR based materials to expand the applications of ECL biosensors based on the cathodic ECL of luminol.

Previous studies showed that the ionic liquids (ILs) could not only interact with GR through covalent and non-covalent interactions to effectively prevent the aggregation of GR sheets (Sun et al., 2016; Zhang et al., 2011b), but also improve the electrochemical performances of the obtained GR-IL nanohybrid materials (Butmee et al., 2019; Zheng et al., 2016; Zhuang et al., 2017). Moreover, the absorbed IL molecules provide sufficient active sites for the nucleation of nanostructured metal materials and act as template to stabilize these materials on the GR-IL matrix (Wang et al., 2016b). On the other hand, the electrochemical properties of materials rely heavily on their nanostructures. Recently, porous materials have aroused extensive interest and attention as a new type of functional materials with an open porous structure, high electric conductivities, large specific surface areas and excellent catalytic activities (Han et al., 2019). So far, these materials have broad application prospects in various field, including catalysts (Fujita et al., 2012; Snyder et al., 2010; Wittstock et al., 2010) and sensors (Banan Sadeghian et al., 2017; Jiang et al., 2018; Zhang et al., 2011a). Take for example the N-(aminobutyl)-N-(ethylisoluminol)-functionalized Ag nanoparticles modified three-dimensional (3D) polyaniline-phytic acid conducting hydrogel (ABEI-Ag@PAni-PA), which was used for in situ sensitive ECL monitoring of H_2O_2 released from live HeLa cells (Jiang et al., 2018). The 3D porous structures benefited a high loading density of the ABEI-Ag luminescent materials and afforded a short diffusion distance to reaction sites for H_2O_2, thus achieving highly sensitive detection.

Herein, an ultrasensitive label-free ECL immunosensor based on cathodic ECL signal of luminol was constructed by using highly porous Pt nanostructures on ionic liquid functionalized graphene film (GR-IL/pPt) composites as a platform for detection of CEA, which was an important biomarker for clinic diagnosis and treatment of cancer (Benchimol et al., 1989; Rizwan et al., 2018a). The as-prepared composites benefited excellent electrocatalytic activity and amplified ECL signal with high loading density of the antibody, thus realizing high sensitivity for CEA detection with a wide linear range and an extremely low detection limit of 0.0003 fg mL^{-1} (S/N = 3). This work proposes a promising platform toward ultrasensitive detection of target analytes in practical applications.

2. Experimental section

2.1. Chemical reagents

Human colon CEA, CEA antibody (anti-CEA), human alpha fetoprotein (AFP), prostate specific antigen (PSA) and human immunoglobulin G (HIgG) were purchased from Linc-Bio Science Co. Ltd. (Shanghai, China). Potassium chloroplatinite (II) (K_2PtCl_4) was obtained from Macklin Biochemical Co., Ltd. (Shanghai, China). 1-butyl-3-methylimidazolium hexafluorophosphate ([BMIM][PF_6]) (≥99%) was obtained from Lanzhou Institute of Chemical Physics, Chinese Academy of Sciences (Lanzhou, China) used as received. Bovine serum albumin (BSA), human serum albumin (HSA), thrombin, luminol and glutaraldehyde (GA) solution (Grade II, 25%) were obtained from Sigma-Aldrich. Chitosan (CHI: MW ca. 100000-300000) was gotten from J&K CHEMICA (Beijing, China). Graphene oxide (GO) (2 mg mL^{-1}) was received from Nanjing XFNANO Materials Tech Co., Ltd (Nanjing, China). Copper(II) sulfate pentahydrate ($CuSO_4{\cdot}5H_2O$), vitamin C (Vc) and glucose were gotten from Sinopharm Chemical Reagent Co., Ltd (Shanghai, China). Phosphate buffered solutions (PBS, pH 7.4) were prepared using 0.1 mol mL^{-1} Na_2HPO_4 and 0.1 mol L^{-1} KH_2PO_4. 5 mL 0.1 M PBS (pH 7.4) containing 0.1 mM luminol and 2 mM H_2O_2 was chosen as the working buffer. All of other reagents were of analytical grade. All of the solutions were prepared by the deionized Millipore Mill-Q water (18.2 MΩ cm).

2.2. Instruments

ECL measurements were carried out on a Model RFL-1 ECL analyzer (Xi'an Remex Instrument Co., Ltd., China) with the voltage of the photomultiplier tube (PMT) set at 500 V and with the auxiliary equipment of CHI 990B electrochemical workstation (Shanghai CH Instruments Co., China). The cyclic voltammetry (CV) and electrochemical impedance spectroscopy (EIS) were performed using a CHI 760 C electrochemical workstation. UV-Vis absorption spectra were obtained using Lambda 750 spectrophotometer (PerkinElmer, USA). Scanning electron microscopy (SEM) (Test parameters: Signal A = Inlens Duo; EHT = 3.0 kV; WD = 5.0 mm) and energy dispersive X-ray spectrum (EDS) were performed with a Gemini microscope (MERLIN Compact, Zeiss Ltd., Germany) equipped with an energy-dispersive X-ray spectrometer. The SEM characterization were carried out on Indium–Tin Oxides (ITO), which were purchased from Kaivo Optoelectronic Technology Co., Ltd (Zhuhai, China).

2.3. Preparation of GR-IL/pPt composite modified electrode

Firstly, GR-IL modified glassy carbon electrode (GCE/GR-IL) was obtained with electrochemical reduction method (Shang et al., 2013). In brief, 0.5 mL of GO solution (1.5 mg mL^{-1}, in ultrapure water) and 0.5 mL of IL ([BMIM][PF_6]) solution (2.5 μL mL^{-1}, in dimethyl formamide (DMF)) were mixed intensively with sonication to gain a uniform GO-IL suspension. Then 4 μL of the suspension was dropped on the pretreated GCE according to the previous method (Li et al., 2018) and dried in the air. Then the as-prepared GCE/GO-IL was immersed into 0.1 M PBS (pH 7.4) followed by scanned for 20 cycles with a potential range from −0.6 to −1.5 V. In this process, GO-IL was reduced to be GR-IL, and the resulting electrode was denoted as GCE/GR-IL. Successively, the porous Pt nanostructures were deposited on the GCE/GR-IL using top-down electrochemical alloying-dealloying technique, by which a more reactive component was selectively removed from an alloy precursor to form the porous structure (Xu et al., 2016). The electrodeposition of Pt-copper (PtCu) bimetals on GCE/GR-IL was performed in 0.1 M KCl solution containing 1 mM K_2PtCl_4 and 40 mM $CuSO_4.5H_2O$ at a constant potential of −0.2 V (vs. Ag/AgCl) for 800 s. The obtained electrode (GCE/GR-IL/PtCu) was washed carefully with ultrapure water, and subsequently subjected to repeated cyclic potential scan (about 20 circles) between −0.2 and 1.2 V in a 0.5 M H_2SO_4 solution until a stable cyclic voltammogram (CV) was obtained. In this case, the more reactive Cu was removed to get GCE/GR-IL/pPt. For comparison, GCE/GR-IL/Pt was fabricated through the similar method without $CuSO_4.5H_2O$ and dealloying process.

2.4. Fabrication of the label-free ECL immunosensor

The fabrication process of the ECL immunosensor was shown in Scheme 1. Firstly, 5 μL of 0.1 mg mL^{-1} CHI solution was dropped onto GCE/GR-IL/pPt and dried in the air to immobilize GR-IL/pPt onto the electrode because of its biocompatibility and film-forming properties (Rizwan et al., 2019). Furthermore, the amine groups are suitable to attach antibody (Stobiecka et al., 2016; Stobiecka and Hepel, 2011; Xu et al., 2011). Then the modified electrode was incubated with 5 μL of 2.5% GA solution at 37 °C for 40 min to sufficiently cross-link CHI and anti-CEA (Ab). After careful washing with ultrapure water, 5 μL of 20 μg mL^{-1} Ab solution was dropped onto the electrode surface

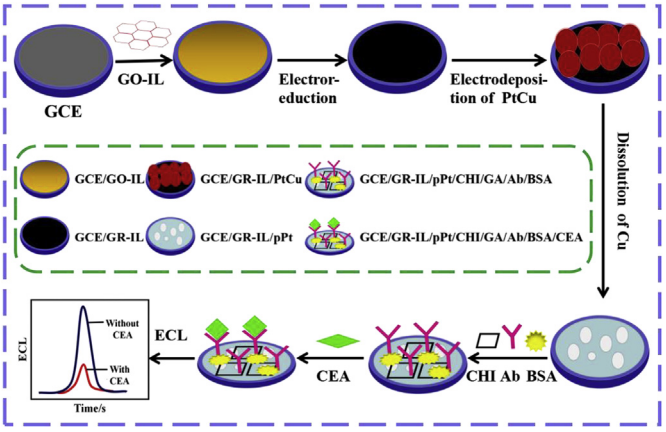

Scheme 1. The fabrication process of ECL immunosensor.

followed by incubated overnight at 4 °C to get GCE/GR-IL/pPt/CHI/GA/Ab. Successively, 5 μL of 1% BSA was incubated on the modified electrode surface to block nonspecific sites for 1 h at 37 °C. After rinsed with 0.1 M PBS buffer (pH 7.4), the label-free ECL immunosensor was fabricated for the detection of CEA and stored at 4 °C until use.

2.5. ECL measurement of CEA

For the detection of CEA, the final ECL immunosensor was incubated with different concentrations of CEA at 37 °C for 2 h. After washed by 0.1 M PBS buffer (pH 7.4), the ECL detection was carried out on a Model RFL-1 ECL analyzer in detector cells containing 5 mL PBS (pH 7.4) with 0.1 mM luminol and 2 mM H_2O_2. The voltage of PMT was maintained at 500 V and the working potential ranged from 0.3 to −0.2 V with a scan rate of 0.1 V s^{-1}.

3. Results and discussion

3.1. Characterization of the GR-IL/pPt composit

It was reported that IL could be interacted with GO, facilitating the preparation of well-dispersed GR with excellent performance (Acik et al., 2012; Fu et al., 2013). Besides, electrochemical reduction method was green and fast to synthesize GR sheets, which displayed better properties than those of through chemical reduction (Guo et al., 2009; Zhou et al., 2009). Therefore, in this work, the electrochemical method was employed to prepare GR-IL film using GO-IL uniform suspension as the starting material. UV-Vis spectra (Fig. S1) confirmed the formation of GO-IL intercalation compounds through the electrostatic and π–π stacking interactions. The electrochemical reduction was characterized by the CVs. As can be seen in Fig. S2A, GCE/GO-IL showed a large reduction current due to the reduction of the surface oxygen groups (Guo et al., 2009). In the successive cycles, this cathodic current decreased considerably and stabilized gradually, demonstrating a quick and irreversible reduction of surface-oxygenated species on GO. The resulted GR-IL film presented typical wrinkled sheet structures intrinsic to GR nanosheets (Chen et al., 2011) (Fig. 1A).

Then porous Pt nanostructures were modified on GR-IL film using top-down electrochemical alloying-dealloying technique (Xu et al., 2016). Firstly, bimetal PtCu nanomaterials were grown in situ on the GR-IL film by electrochemical co-deposition of Pt and Cu from their precursor solutions, showing particle sizes ranging from 100 to 200 nm (Fig. S2B). Then the PtCu was scanned in a potential range from −0.2–1.2 V by several cycles. The first cycle exhibited a large anodic peak at 0.3 V, resulting from the oxidation of Cu (Fig. S2C, curve a). After 20 cycles (Fig. S2C, curve b), the anodic peak disappeared and the hydrogen adsorption/desorption and reduction peaks were very similar to those of GR-IL/Pt (Zhang et al., 2016), indicating the dissolution of Cu atoms and the formation of a Pt shell. As can be seen in Fig. 1B, the remaining Pt showed highly nanoporous structures with pores in the range of a few tens to 200 nm randomly distributed on GR-IL film. Furthermore, the formation of nanoporous Pt was further characterized by EDS analysis (Fig. S3). The results showed that the Cu content decreased greatly after dealloying process, indicating most of Cu atoms were leached out during potential cycling, and thus conforming the formation of porous Pt. For comparison, Pt NPs were also electrodeposited on the surface of GR-IL film (Fig. 1C). Compared with Pt NPs, the nanoporous structures implied a larger specific surface area, which was confirmed by the following electrochemical characterization.

The CV scanning of the GCE/GR-IL/pPt was performed in 0.5 M H_2SO_4 solution at a potential range from −0.2–1.2 V, with GCE/GR-IL/Pt as the control electrode (Fig. 1D). The peaks at about 0.5 V were associated with the reduction of oxide species of Pt for both electrodes, and the reduction peak of GCE/GR-IL/pPt was larger, meaning the presence of more active Pt sites. In addition, the electrochemically active surface areas (ECSAs) of these both electrodes were estimated in Supporting Information using the hydrogen adsorption/desorption peaks (Xu and Lin, 2007). In this case, the ECSA of GCE/GR-IL/pPt was much higher than that of GCE/GR-IL/Pt, facilitating further electrocatalysis and immobilization of antibody.

3.2. ECL performance of GR-IL/pPt composites

The ECL behavior of GR-IL/pPt composite was evaluated in 0.1 M PBS containing 0.1 mM luminol and 2 mM H_2O_2 with bare GCE, GR-IL and GR-IL/Pt as control. As can be seen in Fig. 2A, no detectable ECL emission was observed on the bare GCE. However, the GR-IL modified electrode showed an enhanced cathodic ECL signal, ascribed to the excellent electrical conductivity and electrocatalytic activity of graphene toward the reduction of H_2O_2 to generate the reactive oxygen species (ROSs) such as hydroxyl radical (HO·), which could accelerate the reaction of luminol to form excited 3-aminophthalate anions and thus enhance the cathodic ECL intensity of luminol (Xu et al., 2011). After Pt NPs were electrodeposited on the GR-IL film, the cathodic ECL intensity was further improved. This may be due to the remarkably enhanced electrocatalytic activity of GR-IL/Pt composites, resulting from the quite effective reduction of H_2O_2 from Pt NPs and the synergistic effects provided by GR-IL and Pt NPs (Zhang et al., 2014, 2016), which hastened the formation of ROSs. Surprisingly, GR-IL/pPt composite exhibited an obviously stronger cathodic ECL intensity (~3 fold) than GR-IL/pPt. The reasons may be that the porous structure of pPt with a large pore volume and specific surface area was favorable for exposing more catalytic active sites of Pt and facilitating the mass transfer of reactants by reducing their diffusion path length (Hu et al., 2019), resulting in a higher catalytic efficiency H_2O_2 to generate more ROSs, and thus leading to a considerably improved ECL signal.

To further identify the superior ECL performance, the electrochemical responses of these modified electrodes toward H_2O_2 were investigated. As shown in Fig. 2B, compared with GCE, GCE/GR-IL and GCE/GR-IL/Pt, GCE/GR-IL/pPt exhibited a positively shifted onset potential and a higher peak current for H_2O_2 reduction. The results confirmed that the porous structures promoted the reduction of H_2O_2 to significantly amplify the cathodic ECL response of luminol, implying a promising platform to construct a sensitive label-free ECL immunosensor for the detection of CEA.

3.3. Feasibility of the ECL immunosensor in CEA detection

The electrochemical characterization of the each step in the construction of immunosensor was performed by EIS (Fig. 2C). Compared with the bare electrode (curve a), the GCE/GR-IL/pPt (curve b) showed a very small electron transfer resistance (R_{et}) because of its excellent electrical conductivity. After modified with Ab, an obvious increment of

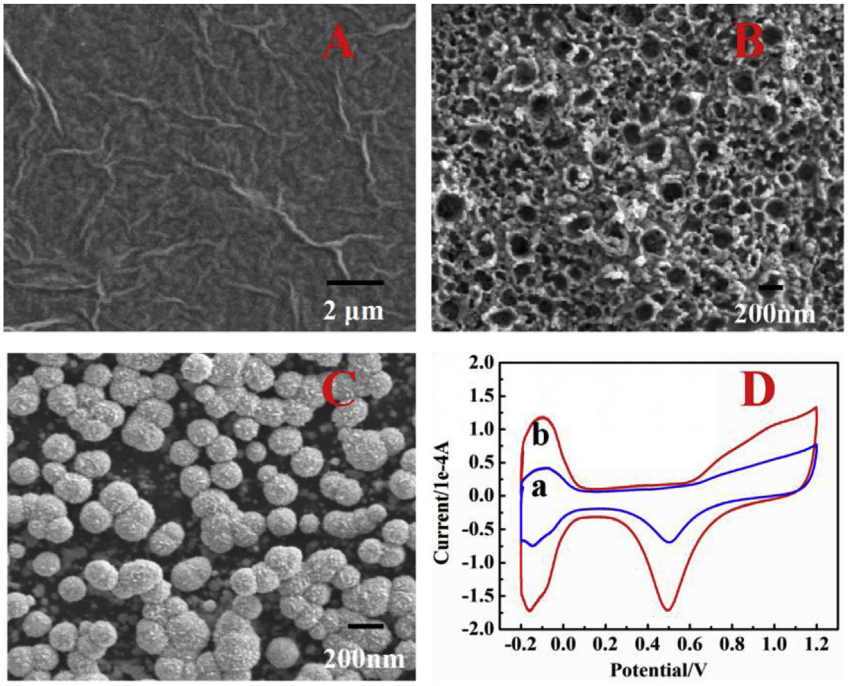

Fig. 1. SEM images of ITO/GR-IL (A), ITO/GR-IL/pPt (B), ITO/GR-IL/Pt (C), and CVs of GCE/GR-IL/Pt (a) and GCE/GR-IL/pPt (b) in 0.5 M H_2SO_4 (D).

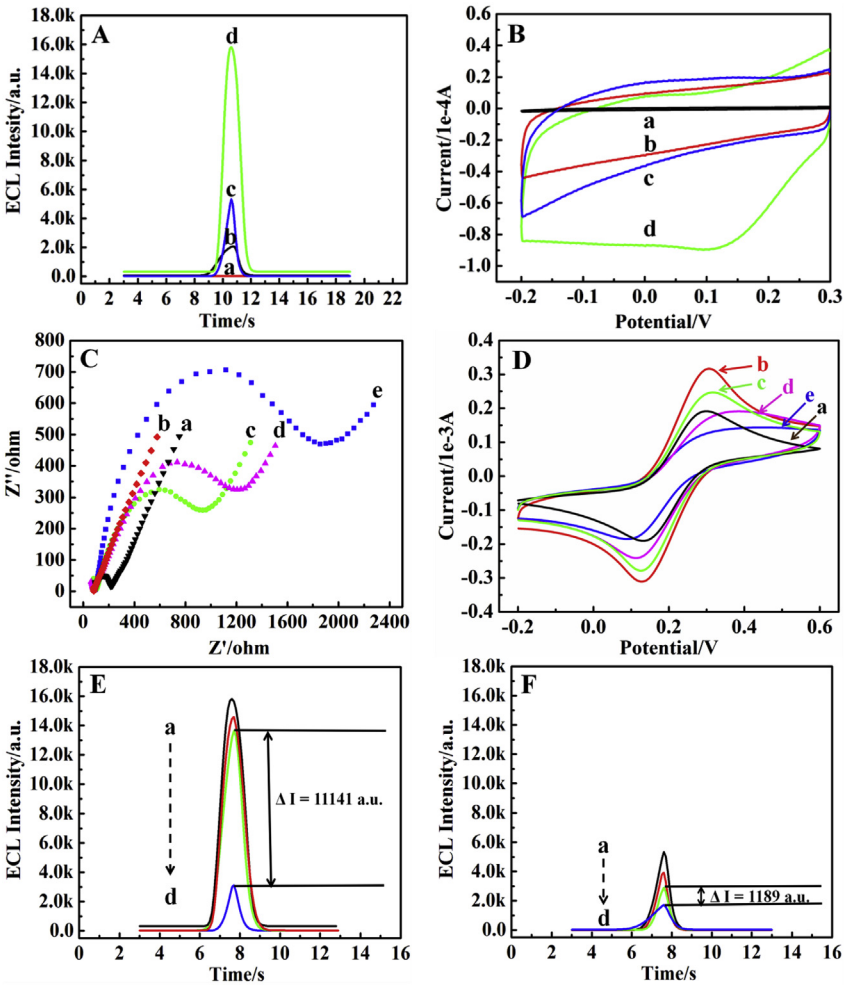

Fig. 2. (A) ECL signal-time curves and (B) CVs of bare GCE (a), GCE/GR-IL (b), GCE/GR-IL/Pt (c), GCE/GR-IL/pPt (d) in 0.1 M PBS (pH 7.4) with 0.1 mM luminol and 2 mM H_2O_2 in the scanning potential range from 0.3 V to −0.2 V with the scan rate of 100 mV s^{-1}. (C) EIS and (D) CV characterization of the different electrodes in 0.1 M KCl containing 5 mM $[Fe(CN)6]^{3-/4-}$: bare GCE (a), GCE/GR-IL/pPt (b), GCE/GR-IL/pPt/CHI/GA/Ab (c), GCE/GR-IL/pPt/CHI/GA/Ab/BSA (d) and GCE/GR-IL/pPt/CHI/GA/Ab/BSA/CEA (e). Frequency range: 0.01–100,000 Hz; Amplitude: 5 mV; Scan rate: 100 mV s^{-1}. (E) and (F) The ECL responses of GCE/GR-IL/pPt (E, a) and GCE/GR-IL/Pt (F, a) after modified with different substances: Ab (b), BSA (c) and 100 pg mL^{-1} CEA (d) in pH 7.4 PBS buffer containing 0.1 mM luminol and 2 mM H_2O_2.

R_{et} was achieved due to the hindered electron transfer by the antibody (curve c). Followed by employing BSA to block the residual nonspecific binding sites, a successive increase of the R_{et} was observed (curve d), attributing to the inhibitory effect of BSA as the inert electron layer (Xiao et al., 2014). Subsequent incubation by CEA resulted in the further increase of the R_{et} (curve e) by the obstacle of the electron transfer from the insulating performance and steric hindrance effect of antibody-antigen complex (Zhu et al., 2017). Therefore, the EIS results indicated that the immunosensor was successfully fabricated. The results were consistent with the CV profiles in Fig. 2D. The GCE/GR-IL/pPt (curve b) showed a higher redox peak current than that of bare GCE (curve a), owing to its excellent conductivity and high surface area. After the Ab, BSA and CEA were modified on the surface of electrode successively, the redox peak current decreased orderly because the bioactive substances greatly inhibited the efficiency of electron transfer. Furthermore, the fabrication process was characterized by SEM, which was discussed in detail in Fig. S4. These results indicated that the immunosensor was successfully fabricated.

To estimate the ECL feasibility of the as-prepared immunosensor, the ECL performance was detected using different modified electrodes (Fig. 2E and F). After the antibody and BSA were successively immobilized, the GCE/GR-IL/pPt and GCE/GR-IL/Pt exhibited an obvious ECL decrease (curve b and c) because of the obstructed electron transfer and the steric hindrance effect by protein molecules. Followed by incubation with CEA antigen, the ECL signal further declined (curve d) thanks to the less conductive immunocomplex, showing the successful detection for CEA. It was worth noting that the ECL decrease on GCE/GR-IL/pPt was much larger than that on GCE/GR-IL/Pt, indicating a greater sensitivity. In this case, on the one hand the pPt nanostructures displayed a better catalytic performance than Pt NPs toward H_2O_2, promoting the cathodic ECL response of luminol; on the other hand, they offered a larger surface area for improving the loading of Ab followed by more amount of incubated CEA, thus greatly enlarging the ECL decrease. Therefore, the GCE/GR-IL/pPt was used as a platform for construction of ECL sensor.

3.4. Performance of the immunosensor in CEA detection

To estimate its analytical performance, the as-proposed ECL immunosensor was explored for the detection of CEA under the optimized experimental conditions (Fig. S5). After incubated with different concentrations of CEA, the ECL responses were collected in Fig. 3A. Thanks to the less conductive immunocomplex, the ECL intensity decreased gradually with the increasing concentration of CEA, and the calibration plot illustrated a good linear relationship between the ECL signals and the logarithm of the concentrations of CEA in a range from 0.001 fg mL^{-1} to 1 ng mL^{-1}. The linear regression equation was $I = -1080.9 \log c + 8827.2$ with a correlation coefficient of 0.99891. The detection limit for CEA was calculated to be 0.0003 fg mL^{-1} (the detailed computing method of LOD was presented in the Supporting Information). The results demonstrated that the proposed label-free ECL immunosensor is highly sensitive and promising to detect CEA. Moreover, compared with other reported sensors for CEA detection (Table 1), the developed ECL immunosensor in our work represented excellent analytical performance with a lower detection limitation and a wider linear range.

3.5. Stability, reproducibility and specificity of the constructed ECL immunosensor

The stability played crucial role in the performance of the prepared immunosensor, and it was measured by ten successively detection of 100 fg mL^{-1} CEA (Fig. 3B). The obtained ECL response did not show any significant changes and the relative standard deviation (RSD) was 0.85%, exhibiting an excellent stability in the CEA detection. Furthermore, six identical modified electrodes were prepared independently under the same experimental conditions and the collected ECL intensities of the six immunosensors showed no obvious fluctuation with a low RSD of 2.30% (Fig. 3C), meaning a superior reproducibility. In short, the proposed immunosensor had good stability and reproducibility.

The specificity of the immunosensor also has an important impact on the analysis of biological samples. Therefore, it was assessed by employing Vc, HSA, glucose, thrombin, AFP, PSA and HIgG as interfering substances. The concentrations of Vc, HSA, glucose, AFP, PSA and HIgG were all 10 ng mL^{-1} with thrombin concentration of 3.74 ng mL^{-1}, which were much higher than that of CEA (10 pg mL^{-1}). As can be seen in Fig. 3D, the ECL signal of the interfering proteins

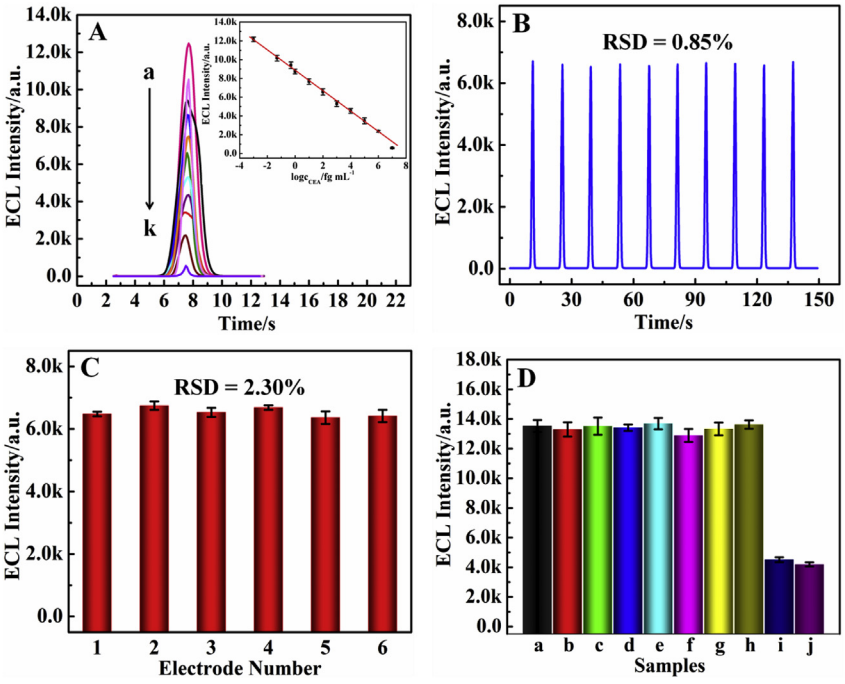

Fig. 3. (A) The ECL intensities of the proposed ECL immunosensor with different CEA concentrations (from a to k: 0.001,0.05, 0.5, 1, 10, 10^2, 10^3, 10^4, 10^5, 10^6 and 10^7 fg mL^{-1}). Inset: the calibration plot between ECL intensities and log c_{CEA}. (B) Stability of the proposed ECL immunosensor with the CEA concentration of 100 fg mL^{-1} undergo consecutive cyclic potential scans for 10 cycles. (C) Reproducibility of the ECL immunosensor with six identical modified electrodes at 100 fg mL^{-1} CEA. (D) Selectivity of the ECL immunosensor toward blank (a), 10 ng mL^{-1} HSA (b), 10 ng mL^{-1} glucose (c), 3.74 ng mL^{-1} thrombin (d), 10 ng mL^{-1} Vc (e), 10 ng mL^{-1} AFP (f), 10 ng mL^{-1} PSA (g), 10 ng mL^{-1} HIgG (h), 10 pg mL^{-1} CEA (i) and mixture (j) (containing all the above analytes). All average ECL intensities were obtained by the results of 3 experiments.

Table 1
Comparison of Proposed Immunosensor with Other Immunosensors in CEA detection.

Sensing platform	Detection method	Linear range (pg mL^{-1})	Detection limit (pg mL^{-1})	References
Porous AuNPs-TGA /16-MHDA-Ab	FL	2–10^2	1.5	Xing et al. (2017)
Ab_2-GOD@Ce:ZONs-Luminol	ECL	8×10^{-2}–10^5	5.2×10^{-2}	Wang et al. (2016a)
AgNCs@Apt@UiO-66	SPR	10^3–2.5×10^5	3×10^2	Guo et al. (2017)
PAMAM-L-Cys-HGNs-Ab_2	ECL	2×10^{-2}–10^3	6.7×10^{-3}	Zhuo et al. (2014)
Ag NPs@CS-Hemin/rGO–Ab_2	EC	2×10^{-2}–10^5	6.7×10^{-3}	Zhang et al. (2019a)
HGNs-MWCNTs-aptamer	EC	10^{-3}–10^4	8.2×10^{-4}	Mazloum- Ardakani et al. (2019)
pPtNPs-Ab	ECL	10^{-6}–10^3	3×10^{-7}	This work

Table 2
Detection of CEA in human serum samples.

Samples	Proposed method (ng/mL)	ELISA (ng/mL)	Relative error (%) (n = 3)	RSD (%) (n = 3)
1	4.03	3.91	2.18	2.36
2	1.38	1.31	5.38	2.70
3	6.92	7.17	−3.53	0.74

showed no obvious change compared with the blank solution. While, the addition of CEA caused a remarkable ECL decrease, indicating good selectivity and specificity of this sensor toward the CEA detection.

3.6. Analytical application in serum samples

Given the proposed ECL sensor showed good analytical performance, it was explored for detection of CEA in human serum samples to investigate its practical application. The serum samples were provided by Liaocheng People's Hospital, and diluted for one hundred times before used. The determined concentration of CEA with this method were consistent with ELISA (Table 2). The results showed that the relative errors and RSD were at an acceptable range, demonstrating the potentiality of the ECL immunosensor for the clinical determination of CEA in human serum.

4. Conclusions

In summary, GR-IL/pPt composite was prepared and exhibited an amplified cathodic ECL signal of luminol, owing to excellent electrocatalytic activity and highly porous structure. Based on this, an ultrasensitive label-free ECL immunosensor was constructed using the composite as platform, which showed ultra-sensitivity, good selectivity, stability and reproducibility for the detection of CEA. Furthermore, it was successfully applied to real human serum samples. Thus, this work provided a new vision to design high-performance ECL nanomaterials, which exhibited great promising in bioanalysis and early clinical diagnoses of cancer.

Declaration of interests statement

The authors declare that they have no known competing financial interests or personal relationships that could have appeared to influence the work reported in this paper.

CRediT authorship contribution statement

Xiao Wang: Methodology, Conceptualization, Software. **Lei Shang:** Methodology, Conceptualization, Writing - review & editing. **Wei Zhang:** Methodology, Writing - review & editing. **Li-Ping Jia:** Formal analysis, Writing - review & editing. **Rong-Na Ma:** Formal analysis, Writing - review & editing. **Wen-Li Jia:** Writing - review & editing. **Huai-Sheng Wang:** Funding acquisition, Formal analysis, Writing - review & editing, Project administration.

Acknowledgements

This work was financially supported by the National Natural Science Foundation of China (21375055, 21505063, 21405070, 21427808), Natural Science Foundation of Shandong Province (ZR2018BB059, ZR2017BB084, ZR2015BQ007) and the Shandong Tai-Shan Scholar Research Fund.

Appendix A. Supplementary data

Supplementary data to this article can be found online at https://doi.org/10.1016/j.bios.2019.111436.

References

Acik, M., Dreyer, D.R., Bielawski, C.W., Chabal, Y.J., 2012. J. Phys. Chem. C 116 (14), 7867–7873.
Banan Sadeghian, R., Han, J., Ostrovidov, S., Salehi, S., Bahraminejad, B., Ahadian, S., Chen, M., Khademhosseini, A., 2017. Biosens. Bioelectron. 88, 41–47.
Benchimol, S., Fuks, A., Jothy, S., Beauchemin, N., Shirota, K., Stanners, C.P., 1989. Cell 57 (2), 327–334.
Butmee, P., Tumcharern, G., Saejueng, P., Stankovic, D., Ortner, A., Jitcharoen, J., Kalcher, K., Samphao, A., 2019. J. Electroanal. Chem. 833, 370–379.
Cao, Y., Yuan, R., Chai, Y., Liu, H., Liao, Y., Zhuo, Y., 2013. Talanta 113, 106–112.
Chen, L., Tang, Y., Wang, K., Liu, C., Luo, S., 2011. Electrochem. Commun. 13 (2), 133–137.
Dai, H., Lin, Y., Xu, G., Gong, L., Yang, C., Ma, X., Chen, G., 2012. Electrochim. Acta 78, 508–514.
Fu, Y., Zhang, J., Liu, H., Hiscox, W.C., Gu, Y., 2013. J. Mater. Chem. A 1 (7), 2663–2674.
Fujita, T., Guan, P., McKenna, K., Lang, X., Hirata, A., Zhang, L., Tokunaga, T., Arai, S., Yamamoto, Y., Tanaka, N., Ishikawa, Y., Asao, N., Yamamoto, Y., Erlebacher, J., Chen, M., 2012. Nat. Mater. 11, 775.
Guo, C., Su, F., Song, Y., Hu, B., Wang, M., He, L., Peng, D., Zhang, Z., 2017. ACS Appl. Mater. Interfaces 9 (47), 41188–41199.
Guo, H.-L., Wang, X.-F., Qian, Q.-Y., Wang, F.-B., Xia, X.-H., 2009. ACS Nano 3 (9), 2653–2659.
Guo, W., Ding, H., Gu, C., Liu, Y., Jiang, X., Su, B., Shao, Y., 2018. J. Am. Chem. Soc. 140 (46), 15904–15915.
Han, J., Li, C., Lu, Z., Wang, H., Wang, Z., Watanabe, K., Chen, M., 2019. Acta Mater. 163, 161–172.
Hu, J., Shi, Z., Wang, X., Qiao, H., Huang, H., 2019. Electrochim. Acta 302, 216–224.
Jiang, X., Chai, Y., Yuan, R., Cao, Y., Chen, Y., Wang, H., Gan, X., 2013. Anal. Chim. Acta 783, 49–55.
Jiang, X., Wang, H., Yuan, R., Chai, Y., 2018. Anal. Chem. 90 (14), 8462–8469.
Kitte, S.A., Gao, W., Zholudov, Y.T., Qi, L., Nsabimana, A., Liu, Z., Xu, G., 2017. Anal. Chem. 89 (18), 9864–9869.
Li, J.-J., Shang, L., Jia, L.-P., Ma, R.-N., Zhang, W., Jia, W.-L., Wang, H.-S., Xu, K.-H., 2018. J. Electroanal. Chem. 824, 114–120.
Li, X., Wu, D., Ma, H., Wang, H., Wang, Y., Fan, D., Du, B., Wei, Q., Zhang, N., 2019. Biosens. Bioelectron. 131, 136–142.
Ling, J., Zhao, M., Chen, F., Zhou, X., Li, X., Ding, S., Tang, H., 2019. Biosens. Bioelectron. 127, 167–173.
Mayer, M., Takegami, S., Neumeier, M., Rink, S., Jacobi von Wangelin, A., Schulte, S., Vollmer, M., Griesbeck, A.G., Duerkop, A., Baeumner, A.J., 2018. Angew. Chem. Int. Ed. 57 (2), 408–411.
Mazloum-Ardakani, M., Tavakolian-Ardakani, Z., Sahraei, N., Moshtaghioun, S.M., 2019. Biosens. Bioelectron. 129, 1–6.
Qiao, Y., Li, Y., Fu, W., Guo, Z., Zheng, X., 2018. Anal. Chem. 90 (15), 9629–9636.
Rizwan, M., Keasberry, N.A., Ahmed, M.U., 2019. Sens. Bio Sens. Res. 24, 100284.
Rizwan, M., Elma, S., Lim, S.A., Ahmed, M.U., 2018a. Biosens. Bioelectron. 107, 211–217.
Rizwan, M., Mohd-Naim, F.N., Ahmed, U.M., 2018b. Sensors 18 (1), 166.
Rizwan, M., Mohd-Naim, N.F., Keasberry, N.A., Ahmed, M.U., 2017. Anal. Method. 9

(17), 2570–2577.
Shang, L., Zhao, F., Zeng, B., 2013. Electroanalysis 25 (2), 453–459.
Snyder, J., Fujita, T., Chen, M.-W., Erlebacher, J., 2010. Nat. Mater. 9, 904–907.
Stobiecka, M., Chalupa, A., Dworakowska, B., 2016. Biosens. Bioelectron. 84, 37–43.
Stobiecka, M., Hepel, M., 2011. Biosens. Bioelectron. 26 (8), 3524–3530.
Sun, Y., Zheng, H., Wang, C., Yang, M., Zhou, A., Duan, H., 2016. Nanoscale 8 (3), 1523–1534.
Wang, J.-X., Zhuo, Y., Zhou, Y., Wang, H.-J., Yuan, R., Chai, Y.-Q., 2016a. ACS Appl. Mater. Interfaces 8 (20), 12968–12975.
Wang, L., Dong, Y., Zhang, Y., Zhang, Z., Chi, K., Yuan, H., Zhao, A., Ren, J., Xiao, F., Wang, S., 2016b. NPG Asia Mater. 8, e337.
Wang, S., Zhao, Y., Wang, M., Li, H., Saqib, M., Ge, C., Zhang, X., Jin, Y., 2019. Anal. Chem. 91 (4), 3048–3054.
Wittstock, A., Zielasek, V., Biener, J., Friend, C.M., Bäumer, M., 2010. Science 327 (5963), 319.
Xiao, F.-N., Wang, M., Wang, F.-B., Xia, X.-H., 2014. Small 10 (4), 706–716.
Xing, T.-Y., Zhao, J., Weng, G.-J., Zhu, J., Li, J.-J., Zhao, J.-W., 2017. ACS Appl. Mater. Interfaces 9 (42), 36632–36641.
Xu, F., Yang, L.-T., Zhao, F.-Q., Zeng, B.-Z., 2016. Int. J. Electrochem. Sci. 11 (2), 1111–1120.
Xu, L.-L., Zhang, W., Shang, L., Ma, R.-N., Jia, L.-P., Jia, W.-L., Wang, H.-S., Niu, L., 2018. Biosens. Bioelectron. 103, 6–11.
Xu, S., Liu, Y., Wang, T., Li, J., 2010. Anal. Chem. 82 (22), 9566–9572.
Xu, S., Liu, Y., Wang, T., Li, J., 2011. Anal. Chem. 83 (10), 3817–3823.
Xu, Y., Lin, X., 2007. J. Power Sources 170 (1), 13–19.
Zhang, C., Zhang, S., Jia, Y., Li, Y., Wang, P., Liu, Q., Xu, Z., Li, X., Dong, Y., 2019a. Biosens. Bioelectron. 126, 785–791.
Zhang, H., Wang, Z., Zhang, Q., Wang, F., Liu, Y., 2019b. Biosens. Bioelectron. 124–125, 184–190.
Zhang, H., Bo, X., Guo, L., 2016. Electrochim. Acta 201, 117–124.
Zhang, L., Lang, X., Hirata, A., Chen, M., 2011a. ACS Nano 5 (6), 4407–4413.
Zhang, Q., Wu, S., Zhang, L., Lu, J., Verproot, F., Liu, Y., Xing, Z., Li, J., Song, X.-M., 2011b. Biosens. Bioelectron. 26, 2632–2637.
Zhang, Y.-Y., Bai, X.-Y., Wang, X.-M., Shiu, K.-K., Zhu, Y.-L., Jiang, H., 2014. Anal. Chem. 86 (19), 9459–9465.
Zheng, Y., Liu, Z., Zhan, H., Li, J., Zhang, C., 2016. Anal. Method. 8 (26), 5288–5295.
Zhou, M., Wang, Y., Zhai, Y., Zhai, J., Ren, W., Wang, F., Dong, S., 2009. Chem. Eur J. 15 (25), 6116–6120.
Zhu, X., Zhai, Q., Gu, W., Li, J., Wang, E., 2017. Anal. Chem. 89 (22), 12108–12114.
Zhuang, X.-M., Chen, D.-D., Wang, S.-N., Liu, H.-T., Chen, L.-X., 2017. Sensor. Actuator. B Chem. 251, 185–191.
Zhuo, Y., Gui, G., Chai, Y., Liao, N., Xiao, K., Yuan, R., 2014. Biosens. Bioelectron. 53, 459–464.